A Mechanistic Model for Carbon Dioxide Corrosion of Mild Steel in the Presence of Protective Iron Carbonate Films—Part 3: Film Growth Model

S. Nešić,‡, and K.-L.J. Lee***

ABSTRACT

A model of iron carbonate ($FeCO_3$) film growth is proposed, which is an extension of the recent mechanistic model of carbon dioxide (CO_2) corrosion by Nesic, et al. In the present model, the film growth occurs by precipitation of iron carbonate once saturation is exceeded. The kinetics of precipitation is dependent on temperature and local species concentrations that are calculated by solving the coupled species transport equations. Precipitation tends to build up a layer of $FeCO_3$ on the surface of the steel and reduce the corrosion rate. On the other hand, the corrosion process induces voids under the precipitated film, thus increasing the porosity and leading to a higher corrosion rate. Depending on the environmental parameters such as temperature, pH, CO_2 partial pressure, velocity, etc., the balance of the two processes can lead to a variety of outcomes. Very protective films and low corrosion rates are predicted at high pH, temperature, CO_2 partial pressure, and Fe^{2+} ion concentration due to formation of dense protective films as expected. The model has been successfully calibrated against limited experimental data. Parametric testing of the model has been done to gain insight into the effect of various environmental parameters on iron carbonate film formation. The trends shown in the predictions agreed well with the general understanding of the CO_2 corrosion process in the presence of iron carbonate films. The present model confirms that the concept of scaling tendency is a good tool for predicting the likelihood of protective iron carbonate film formation.

KEY WORDS: carbon dioxide, carbon dioxide corrosion, carbon steel, model, prediction, protective films

INTRODUCTION

The recent mechanistic model of Nesic, et al.,[1] covers most of the important processes present in uniform carbon dioxide (CO_2) corrosion of carbon steel: electrochemical reactions at the steel surface, chemical reactions and transport of species between the steel surface, and the bulk solution including transport through the porous corrosion film. The physical, mathematical, and numerical aspects of the model are explained in detail in the original paper; however, a brief outline is given below to facilitate the understanding of the present model.

Since it is a model of uniform corrosion, a one-dimensional computational domain is used, stretching from the steel surface through the pores of a surface film and the mass-transfer boundary layer, ending in the turbulent bulk of the solution, as sketched in Figure 1. The concentration of each species is governed by a species conservation (mass balance) equation. A universal form of the equation, which describes transport for species j in the presence of chemical reactions, which is valid both for the liquid boundary layer and the porous film, is:[1-2]

Submitted for publication January 2002; in revised form, March 2003. Presented as paper no. 01040 at CORROSION/2001, March 2001, Houston, TX. Part 1 of this manuscript appears in *Corrosion* 59, 5 (2003), p. 443. Part 2 appears in *Corrosion* 59, 6 (2003), p. 489.

‡ Corresponding author

* Department of Mechanical Engineering, The University of Queensland, Brisbane Queensland, Australia. Present address: Institute for Corrosion and Multiphase Flow Technology, Chemical Engineering Department, Ohio University, 340 1/2 W. State St., Stocker Center, Athens, OH 45701. E-mail: nesic@bobcat.ent.ohiou.edu.

** Department of Mechanical Engineering, The University of Queensland, Brisbane Queensland, Australia.

0010-9312/03/000123/$5.00+$0.50/0

$$\underbrace{\frac{\partial(\varepsilon c_j)}{\partial t}}_{\text{accumulation}} = \underbrace{\frac{\partial}{\partial x}\left(\varepsilon^{1.5} D_j^{\text{eff}} \frac{\partial c_j}{\partial x}\right)}_{\text{net flux}} + \underbrace{\varepsilon R_j}_{\substack{\text{source or sink} \\ \text{due to chemical reactions}}} \quad (1)$$

where c_j is the concentration of species j in kmol m^{-3}, ε is the porosity of the film, D_j^{eff} is the effective diffusion coefficient of species j (which includes both the molecular and the turbulent component) in $m^2\ s^{-1}$, R_j is the source or sink of species j due to all the chemical reactions in which the particular species is involved in kmol $m^{-3}\ s^{-1}$, t is time, and x is the spatial coordinate in m.

It should be noted that in the transport equation above electromigration has been neglected as its contribution to the overall flux of species is small. Turbulent convection has been replaced by turbulent diffusion as the former is difficult to determine explicitly in turbulent flow. A well-established statistical technique is used instead: instantaneous velocity is divided into the steady and the turbulent-fluctuating components. Close to a solid surface, the steady velocity component is parallel to the surface and does not contribute to the transport of species in the direction normal to the metal surface. The turbulent convection term can be approximated by a "turbulent diffusivity" term,[3] $-D_t\, \partial c_j / \partial x$, and lumped with the molecular viscosity term to give D_j^{eff}. The turbulent diffusion coefficient, D_t, is a function of the distance from the metal or solid film surface and is given by:[3]

$$D_t = \begin{cases} 0 & \text{for } x < \delta_f \\ 0.18\left(\dfrac{x-\delta_f}{\delta-\delta_f}\right)^3 \dfrac{\mu}{\rho} & \text{for } x > \delta_f \end{cases} \quad (2)$$

The liquid boundary layer thickness is typically a function of the Reynolds number. For pipe flow it reads:[3]

$$\delta - \delta_f = 25\,\mathrm{Re}^{-7/8}\, d \quad (3)$$

where d is the hydraulic diameter in m, $\mathrm{Re} = \rho U d/\mu$ is the Reynolds number, U is bulk velocity in m s^{-1}, ρ is the density in kg m^{-3}, and μ is dynamic viscosity in kg $m^{-2}\ s^{-1}$. It is assumed that there is no fluid flow within the porous film (for $x < \delta_f$).

When species j is involved in k chemical reactions simultaneously, one can write for the source/sink term in Equation (1):

$$R_j = a_{jk} r_k \quad (4)$$

where tensor notation applies for the subscripts, a_{jk} is the stoichiometric matrix where row j represents the j-th species, column k represents the k-th chemical reaction, and r_k is the reaction rate vector. A

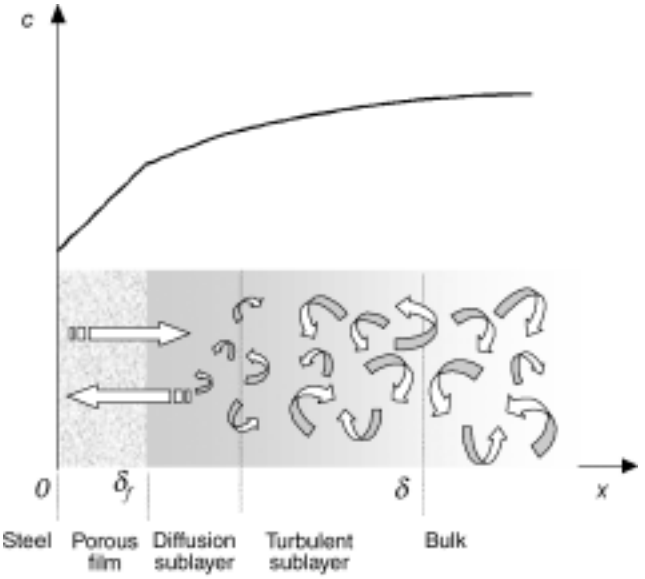

FIGURE 1. *Sketch of the computational domain and a typical concentration profile for a dissolved species.*

chemical reaction of special interest is iron carbonate precipitation, which has been implemented in the model as taking place at the steel surface, in the porous corrosion film, and on the existing film surface. The precipitation reaction acts as a sink for Fe^{2+} and CO_3^{2-} ions, influencing the fluxes and concentration gradients for both the ions and all other carbonic species. It is described in more detail in the heading below.

A transport equation (1) is written for each species. They all have to be solved simultaneously in space and time. The boundary conditions for this set of partial differential equations are the following:

—in the bulk: equilibrium concentrations of species (which is also used as the initial condition);

—at the steel surface: a flux of species is determined from the rate of the electrochemical reactions (zero flux for non-electroactive species).

Even if the original model of Nesic, et al.,[1] described briefly above, is mechanistic and offers an insight into the various complex processes occurring in CO_2 corrosion, from a practical point of view it is just another worst-case CO_2 corrosion prediction model. Admittedly, it does go one step further than other similar CO_2 models as it enables prediction of conditions leading to protective film formation, as well as the effect of protective films, *once they are in place*. However, there is a missing link: it cannot predict the kinetics of film growth, nor can it predict the morphology of the growing films. The present study aims at filling these gaps (i.e., it uses the mechanistic model of Nesic, et al.,[1] as a basis and extends it to cover the film growth process).

In the text following, the physical mathematical and numerical aspects of the film growth model are

discussed first. This is followed by a section discussing the verification of the model done by comparing the predictions with measurements. Finally, a section is included where the new model is used to study the effects of various parameters affecting the film growth process and the effects on the corrosion rate.

FILM GROWTH MODEL

In CO_2 corrosion of carbon steel, when the concentrations of Fe^{2+} and CO_3^{2-} ions exceed the solubility limit, they can precipitate to form solid iron carbonate according to:

$$Fe^{2+} + CO_3^{2-} \Rightarrow FeCO_{3(s)} \quad (5)$$

When iron carbonate precipitates at the steel surface, it can slow down the corrosion process by presenting a diffusion barrier for the species involved in the corrosion process but also by blocking (covering) a portion of the steel surface and preventing the underlying steel from further dissolution.

Iron carbonate film growth depends primarily on the precipitation rate, R_{FeCO_3}. As more iron carbonate precipitates, the film grows in density as well as thickness. However, the steel surface corrodes under the film, continuously creating a "void" between the film and the steel surface (hereafter called "film undermining"). As soon as it is created, the void starts filling up by the ongoing precipitation. When the rate of precipitation at the steel surface equals or exceeds the rate of corrosion (film undermining), dense protective films form—sometimes very thin but still protective. Vice versa, when the corrosion process undermines the newly formed film faster than precipitation can fill in the voids, a porous and unprotective film forms, which can be sometimes very thick and still unprotective. This phenomenon has been previously quantified through the use of a non-dimensional parameter termed "scaling tendency":[4]

$$ST = \frac{R_{FeCO_3}}{CR} \quad (6)$$

which describes the relative rates of precipitation and corrosion expressed in the same volumetric units. For ST<<1, porous and unprotective films are likely to form. Conversely, when ST≥1, conditions become favorable for formation of dense, protective iron carbonate films. However, the use of scaling tendency is not as straightforward as it appears. Strictly speaking, one needs to compute the scaling tendency at the steel surface where the films form (surface scaling tendency [SST]). Therefore, one needs information about the solution chemistry at the steel surface, which can be very different from the one in the bulk, particularly if some sort of surface film is already in place (e.g., iron carbide, mill scale). Further, the scaling tendency changes with time as the corrosion and precipitation rates change. It should be stressed that the model shown below does not explicitly use the concept of scaling tendency, even if the physical processes underlying it (precipitation and undermining) are accounted for. The surface and bulk scaling tendencies are computed in the model to check their validity as effective indicators of protective film formation.

The proposed equation describing the film growth kinetics is rather simple. As $FeCO_3$ is just another species in the system, a mass balance can be written in the same form (Equation [1]) as is done for other species:

$$\underbrace{\frac{\partial c_{FeCO_{3(s)}}}{\partial t}}_{\substack{\text{local}\\ \text{change}}} = \underbrace{R_{FeCO_{3(s)}}}_{\substack{\text{precipitation}\\ \text{rate}}} \quad (7)$$

Note that the transport term has been dropped as $FeCO_3$ is a solid and therefore its diffusion and convection can be neglected. The equation expresses the fact that the amount (concentration) of solid iron carbonate found in any volume, $c_{FeCO_{3(s)}}$ (in kmol m^{-3}), will increase over time if there is precipitation.

However, as discussed above, the corrosion process removes the steel under the film, which in mathematical terms is equivalent to the steel surface shown in Figure 1 moving to the left (i.e., away from any existing film). Within the framework of a fixed (in space) computational domain, this is a moving boundary problem. If the whole domain is to be covered at all times, it appears that a computational domain (grid) needs to be continuously extended to the left to "cover" the voids created by the corrosion process. This is not easy and would require a lot of interpolation and complex bookkeeping. Another simpler option is to assume that the computational grid is "attached" to the steel surface that is moving to the left with a velocity equal to the corrosion rate, CR. The advantage of this option is that, in this case, one does not have to keep extending the grid but can operate with the same grid (which is moving). The whole computational domain, including the film shown in Figure 1 (which does not move), appears to move to the right in a moving frame of reference, as corrosion proceeds. In other words, a convective-like term appears in all the transport equations (Equation [1]) for the species as well as in Equation (7) for solid iron carbonate. This term appears to be sweeping everything away from the steel surface with a velocity CR that has the same effect as the surface of the steel moving in the opposite direction with the same velocity. Hence, the convective-like term appears on

the right-hand side of Equation (7), describing the film-undermining effect:[1]

$$\underbrace{\frac{\partial c_{FeCO_{3(s)}}}{\partial t}}_{\substack{\text{local}\\ \text{change}}} = \underbrace{R_{FeCO_{3(s)}}}_{\substack{\text{precipitation}\\ \text{rate}}} - \underbrace{CR\frac{\partial c_{FeCO_{3(s)}}}{\partial x}}_{\substack{\text{undermining}\\ \text{rate}}} \quad (8)$$

Another aspect of Equation (8) deserves a comment. Physically, precipitation of crystalline films (such as iron carbonate) goes through two phases: nucleation and crystal growth.[5] In most cases when there is a solid steel surface present, with all its imperfections being good candidates for nuclei formation, the nucleation phase is over relatively fast and can be disregarded. It can be assumed that the rate of precipitation is controlled by the crystal growth rate. Generally, crystals grow from a large number of discrete nuclei into dendritic structures, which may or may not join, forming a porous film. A discrete lattice growth modeling approach has been used in the past to describe the film growth process.[6-8] However, for the purposes of the present model, it would be computationally costly and mathematically difficult to model a three-dimensional discrete film growth process and couple it to the existing one-dimensional transport model for all the other species. It seemed more appropriate to persist with the one-dimensional control volume approach in describing the film growth as expressed by Equation (8). In a control volume approach, all properties are assumed to be constant within a control volume and therefore it appears that some detailed information about the film can be lost—smeared over the control volume. This can be avoided by using very fine grids—small control volume sizes on the order of $\Delta x \propto 10^{-7}$ m, which are still a few orders of magnitude larger than the length scale of the dendrites. In this way, it can be assumed that any averaging of the film properties across such small control volumes will not lead to a significant loss of detailed information. After all, the present model is not aimed at elucidating the fine points of crystalline iron carbonate film growth, but attempts to capture the overall effect these films have on the CO_2 corrosion process.

It is convenient to express the morphology of iron carbonate films via the distribution of volumetric porosity (ε) since it is used as the principal film parameter affecting transport of species. Tortuosity and permeability of the film, which appear in the original transport equation, already have been expressed in terms of porosity (Equation [1]).[1] Recall that volumetric porosity is defined as:

$$\varepsilon = \frac{V_{void}}{V_{total}} = \frac{(V_{total} - V_{FeCO_{3(s)}})}{V_{total}} = 1 - \frac{V_{FeCO_{3(s)}}}{V_{total}} = 1 - \frac{c_{FeCO_{3(s)}} M_{FeCO_{3(s)}}}{\rho_{FeCO_{3(s)}}} \quad (9)$$

where $M_{FeCO_{3(s)}} = 115.847$ kg kmol^{-1} is the molecular mass and $\rho_{FeCO_3} = 3{,}900$ kg m^{-3} is the density of iron carbonate. This relationship between porosity (ε) and iron carbonate concentration ($c_{FeCO_{3(s)}}$) allows the rearrangement of the film growth Equation (8) to be expressed in terms of porosity:

$$\frac{\partial \varepsilon}{\partial t} = -\frac{M_{FeCO_{3(s)}}}{\rho_{FeCO_{3(s)}}} R_{FeCO_{3(s)}} - CR\frac{\partial \varepsilon}{\partial x} \quad (10)$$

The rate of precipitation ($R_{FeCO_{3(s)}}$) in Equation (10) can be described as a function of supersaturation (S), the solubility limit (K_{sp}), temperature (T), and surface area-to-volume ratio (A/V):[9]

$$R_{FeCO_{3(s)}} = \frac{A}{V} \times f(T) \times K_{sp} \times f(S) \quad (11)$$

Supersaturation is defined as:

$$S = \frac{c_{Fe^{2+}} c_{CO_3^{2-}}}{K_{sp}} \quad (12)$$

From the two different expressions describing the kinetics of iron carbonate precipitation proposed by Johnson and Tomson[9] and van Hunnik, et al.,[4] the latter is used in conjunction with the film growth model because it is believed to give more realistic results especially at higher supersaturation.

Within the context of the present model, the surface area-to-volume ratio (A/V) is defined locally—as a function of the film porosity in a particular control volume. The two studies mentioned above offered no guidance on what values for A/V to use in such a case.[4,9] Using simple asymptotic analysis, it can be deduced that in the bulk solution where there is no film, ε = 1 and A/V = 0. Implicitly this means that homogeneous precipitation in the bulk solution does not occur no matter how high the local supersaturation and temperature. On the other end of the ε scale, in 100% dense films, ε = 0 and A/V = 0. In between these extremes, for $0 < \varepsilon < 1$, the surface area-to-volume ratio can become very large. There is some information in the open literature on how A/V changes with porosity[10-11] based on simple geometri-

[1] The sweeping effect is not very significant for transport of the dissolved species in the solution (described by Equation [1]) as the sweeping velocity CR is at least a few orders of magnitude smaller than the "diffusional velocity" and neglibible when compared to convection. For example, a corrosion rate on the order of 1 mm/y amounts to a sweeping velocity on the order of 1 nm/min. Diffusional velocity for a typical species in the solution is on the order of 1 mm/min.

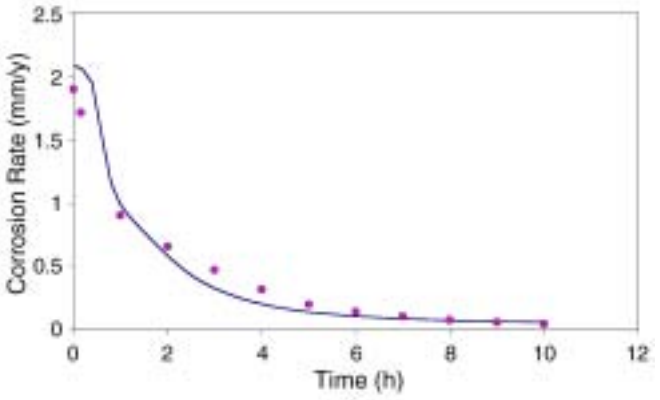

FIGURE 2. *Comparison between experimental data (points) and model predictions (line) for T = 80°C, pH 6.6, P_{CO_2} = 0.54 bar, $c_{Fe^{2+}}$ = 250 ppm, and v = 1 m/s.*

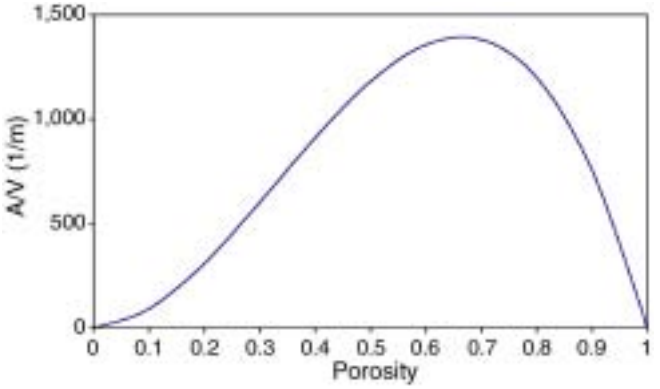

FIGURE 3. *Surface area-to-volume ratio (A/V) as a function of porosity (ε) for a control volume of $\Delta x \propto 10^{-7}$ m.*

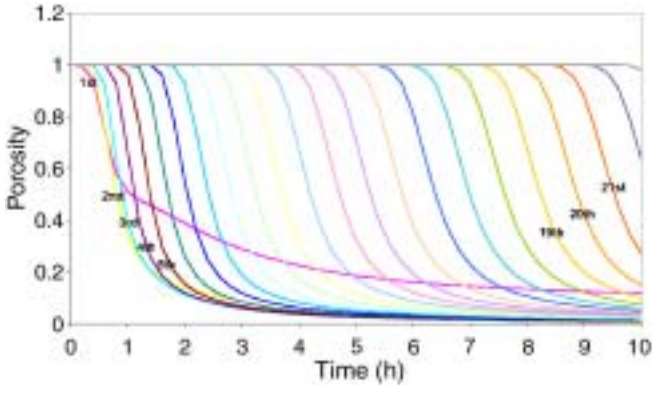

FIGURE 4. *Predicted porosity change of different iron carbonate film layers with respect to time. Each layer is 0.16 μm thick. Conditions: T = 80°C, pH 6.6, P_{CO_2} = 0.54 bar, $c_{Fe^{2+}}$ = 250 ppm, and v = 1 m/s.*

cal models, which usually fail at one of the extremes. After much trial and error, by using geometrical as well as physical arguments, and through comparison with CO_2 corrosion experiments (described below), it has been concluded that the area-to-volume ratio can be expressed as a function of porosity in the following form:

$$\frac{A}{V} \propto \frac{\varepsilon^2(1-\varepsilon)}{\Delta x} \qquad (13)$$

where Δx is the width of the control volume.

NUMERICAL MODEL

The film growth Equation (10) was discretized using a finite difference method. An explicit time discretization scheme was used to simplify the coupling with the rest of the model, which was discretized fully implicitly to maintain stability. This can be justified easily by the wide disparity of the time scales: characteristic time for the species transport equations (Equation [1]) is on the order of seconds while, for the film growth Equation (10), it is on the order of hours or even days. In other words, film precipitation happens so slowly, compared to the other processes in CO_2 corrosion, that it can be calculated by using an explicit time discretization scheme without risking instability.

In Equation (10), the film-undermining term, $CR\partial\varepsilon/\partial x$, is of a convective nature as discussed previously. A first-order upwinding method is commonly used (in lieu of central differences) for spatial discretization of convective terms to achieve numerical stability. However, in the absence of any physical diffusion (iron carbonate films do not diffuse), simple upwinding leads to large numerical diffusion and unacceptable levels of numerical errors. This is due to the hyperbolic nature of Equation (10) and the very small CFL number ($CFL = CR\Delta t/\Delta x \approx 10^{-3}$). Exact solution of hyperbolic equations is obtained only for CFL = 1.[12-13] Therefore, a more accurate Koren's flux limiter scheme[14] was used to discretize the film-undermining term.

A typical initial condition for Equation (10) used below was ε = 1 throughout the solution (i.e., a case with no initial film), although any other porosity profile could have been used instead to simulate the presence of a preformed carbide film or a mill scale. Boundary conditions for Equation (10) were ε = 0 at the steel surface and ε = 1 in the bulk solution.

Results of all the simulations shown below were numerically tested by performing temporal and spatial grid refinement studies. The data shown in all the figures below are all grid and time-step independent (within acceptable tolerances). Uniform control, volume size, and time steps were used to improve the order of accuracy of the interpolation schemes.

COMPARISON WITH EXPERIMENTS

To verify and "fine-tune" the performance of the model described above, accurate CO_2 corrosion ex-

periments in the presence of iron carbonate films were needed. There is a number of such experiments found in the open literature; however, upon closer inspection, all had to be rejected because there was some relevant information that was not reported in each of them. Therefore, custom-designed glass cell experiments were conducted using a rotating cylinder electrode. Conditions were chosen to enable rapid protective iron carbonate film formation in a relatively short time frame (one to two days), so that the reproducibility of the measurements could be easily established.

Experimental Setting and Procedure

The glass cell was filled up with 2.5 L of electrolyte, which was made up of distilled water and 1.0 wt% sodium chloride (NaCl). At the beginning, the solution was deaerated by bubbling CO_2 gas for 1 h. The cell was sealed tightly to prevent oxygen contamination, and CO_2 gas bubbling was continued throughout the experiment; hence, it can be assumed that water vapor and CO_2 were the only gas constituents. Subsequently, the solution was heated to 80°C. Since the cell was operating at atmospheric pressure, partial pressure of CO_2 was approximately 0.54 bar. The desired pH of 6.6 was then adjusted by adding sodium hydrogen carbonate ($NaHCO_3$). A cylindrical 1020 mild steel specimen with a ferritic-pearlitic microstructure was sanded using 1000-grit silicon carbide (SiC) paper, then washed with ethanol (C_2H_5OH), and dried before immersion into the solution. The rotating speed of the cylindrical specimen was adjusted to give a peripheral velocity of the steel surface of 1 m/s. The electrochemical corrosion measurements were performed by using a potentiostat connected to a PC. The corrosion rate was measured every hour using the linear polarization resistance (LPR) method, by polarizing the working electrode ±5 mV vs the open-circuit potential at a rate of 0.1 mV/s. The polarization constant B was determined to be 17 mV by using the simplified electrochemical model of Nešić, et al.[15] This procedure of determining the B value was frequently verified with weight loss and was found to be accurate within ±15%. At the end of the experiment, after the specimen was removed from the cell, it was immediately rinsed with ethanol to avoid film contamination with oxides. It was then allowed to dry and mounted in a low viscosity epoxy resin to fix the film. The specimen was cross-sectioned, polished, platinum-coated, and observed using scanning electron microscopy (SEM) and energy-dispersive spectroscopy (EDS).

Comparison Case #1

In Figure 2, measured and predicted corrosion rates are compared for an experiment conducted at atmospheric pressure, temperature (T = 80°C), pH 6.6, partial pressure of CO_2 (P_{CO_2} = 0.54 bar), and velocity (v = 1 m/s). To form protective $FeCO_3$ films via precipitation in a short time frame, steel wool was placed at the bottom of the glass cell at the very beginning of the experiment to provide an ample source of Fe^{2+} ions. Based on pH 6.26 (measured once the pH reading stabilized with the steel wool in the cell), it was estimated via equilibrium calculations that the bulk concentration of Fe^{2+} was ≈250 ppm, leading to a bulk supersaturation (S = 576) and a surface scaling tendency of SST = 9.7 at the steel surface prior to any film formation. As expected under these conditions, the corrosion rate was reduced rapidly as protective iron carbonate films formed. The experiment was stopped after 10 h when the corrosion rate was <0.03 mm/y. The agreement between measured and predicted values shown in Figure 2 is very good

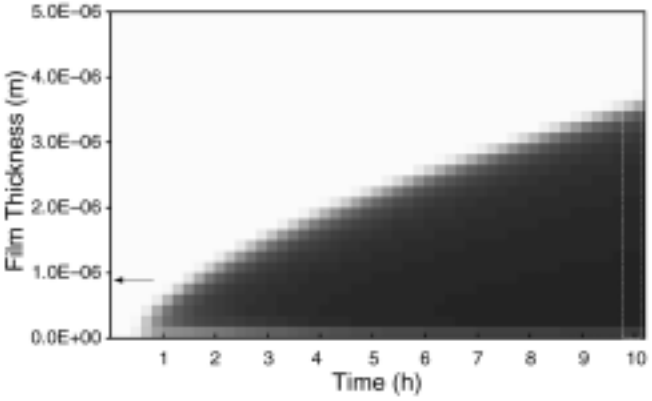

FIGURE 5. *Predicted iron carbonate film growth with respect to time for T = 80°C, pH 6.6, P_{CO_2} = 0.54 bar, $c_{Fe^{2+}}$ = 250 ppm, and v = 1 m/s. Black depicts a 100% dense (ε = 0) iron carbonate film and white means no film (ε = 1). The arrow denotes the position of the steel surface at the beginning of the corrosion process (t = 0). The rectangle highlights the film obtained after 10 h, which is used for comparison with the experimentally observed film shown in Figure 6.*

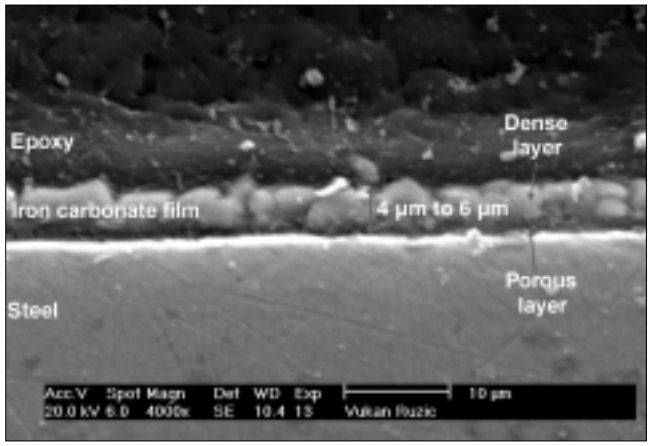

FIGURE 6. *SEM image of a cross section of a steel specimen including an iron carbonate film. Exposed for 10 h at T = 80°C, pH 6.6, P_{CO_2} = 0.54 bar, $c_{Fe^{2+}}$ = 250 ppm, and v = 1 m/s.*

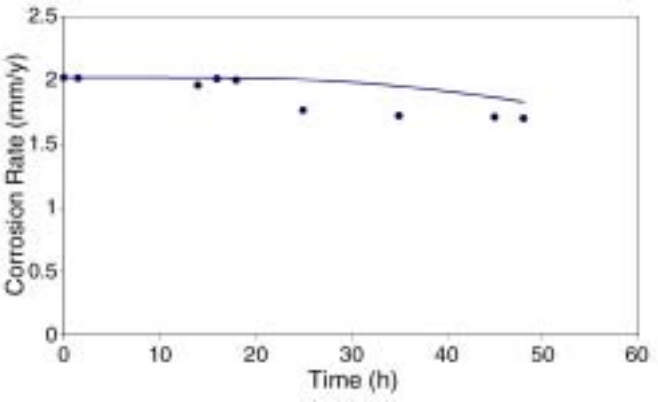

FIGURE 7. *Comparison between experimental data (points) and model predictions (line) for T = 80°C, pH 6.6, P_{CO_2} = 0.54 bar, $c_{Fe^{2+}}$ = 5 ppm, and v = 1 m/s.*

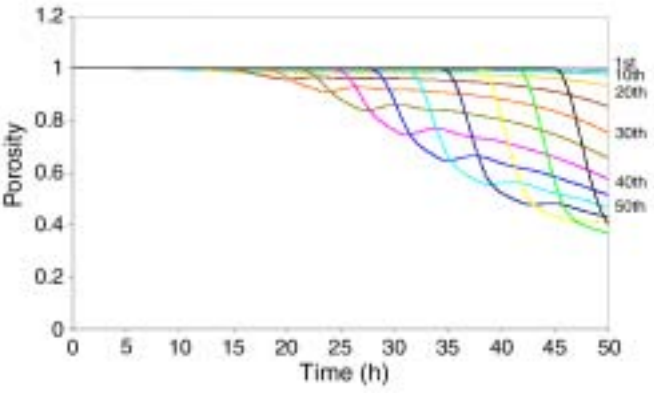

FIGURE 8. *Predicted porosity change of different iron carbonate film layers with respect to time. Each layer is 0.16 μm thick. Conditions: T = 80°C, pH 6.6, P_{CO_2} = 0.54 bar, $c_{Fe^{2+}}$ = 5 ppm, and v = 1 m/s.*

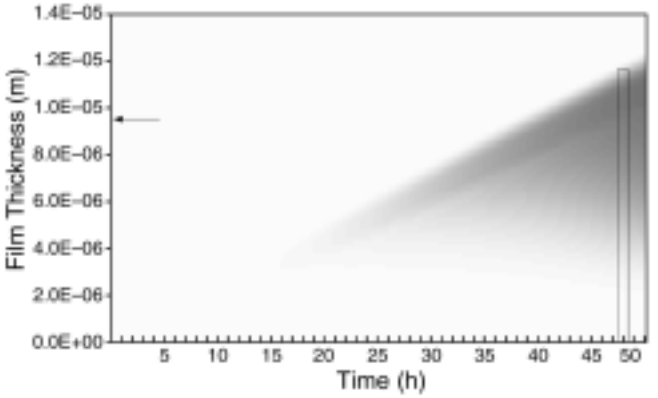

FIGURE 9. *Predicted iron carbonate film growth with respect to time for T = 80°C, pH 6.6, P_{CO_2} = 0.54 bar, $c_{Fe^{2+}}$ = 5 ppm, and v = 1 m/s. Black depicts a 100% dense (ε = 0) iron carbonate film and white means no film (ε = 1). The arrow denotes the position of the steel surface at the beginning of the corrosion process (t = 0). The rectangle highlights the film obtained after 48 h, which is used for comparison with the experimentally observed film shown in Figure 10.*

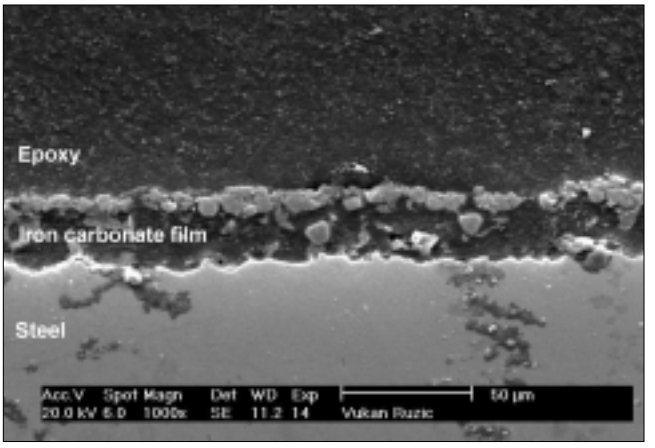

FIGURE 10. *SEM image of a cross section of a steel specimen including an iron carbonate film. Exposed for 48 h at T = 80°C, pH 6.6, P_{CO_2} = 0.54 bar, $c_{Fe^{2+}}$ = 5 ppm, and v = 1 m/s.*

given the complexity of the processes involved. To achieve such agreement, the only freely adjustable parameter in the model was the unknown proportionality constant between the surface area-to-volume ratio and the porosity of the film in Equation (13). The resulting relationship is depicted in Figure 3, suggesting that the internal surface area of the porous film grows rapidly as the film develops, reaching >1,000 m^2/m^3, and then gradually reduces as the pores fill up with iron carbonate.

The predicted film growth process is shown in Figure 4 as a change of porosity in each control volume (layer of the film) with respect to time. It can be seen that the porosity decreases (i.e., film buildup is initially sharpest in the first layer directly adjacent to the steel surface which is to be expected as nucleation can only happen there and because the highest supersaturation is reached at the steel surface). However, as the steel surface corrodes under the film and undermines it, the second layer away from the steel surface experiences fastest film buildup, followed by the third layer, etc., as the film grows in thickness. After 10 h, a very dense and protective film is formed close to the steel surface. Since the bulk supersaturation is very high the film would keep on growing. It is interesting to note that the first layer adjacent to the steel surface never reached the same high density of the other layers above it as a result of the undermining effect by corrosion.

Another probably more intuitive way of looking at the same film growth process is depicted in Figure 5. There, a change of porosity of the film is shown in time and space by using different shades of gray, black depicting a 100% dense (ε = 0) iron carbonate film and white meaning no film (ε = 1). Under the given conditions, the film thickness changes approximately in a parabolic fashion with time as predicted by simple theory; however, this in not always the case, as will be illustrated.

TABLE 1

Predicted Supersaturation, Scaling Tendency, Film Thickness, and Corrosion Rate at Various pH for T = 80°C, P_{CO_2} = 0.54 bar, $c_{Fe^{2+}}$ = 250 ppm, and v = 1 m/s

pH	Supersaturation (prior to any film formation)		Scaling Tendency (prior to any film formation)		Film Thickness[A] (after 30 h) in μm	Corrosion Rate[B] (after 30 h) in mm/y
	Surface	Bulk	Surface	Bulk		
5.8	63	11	0.41	0.06	6.2	1.6
6.0	154	29	1.03	0.18	4.9	0.13
6.26	464	104	3.03	0.66	4.8	0.04
6.6	1,595	576	9.70	3.35	8.4	0.03

[A] Film thickness as well as porosity are shown in Figure 12.
[B] Corresponding corrosion rate vs time curves are shown in Figure 11.

The SEM image of the cross section of the steel specimen from the experiment described above (exposed for 10 h) is shown in Figure 6. When comparing the film thickness and morphology with the predicted values (highlighted by the rectangle in Figure 5), it is seen that the agreement is good for the thickness of film (measured: 4 μm to 6 μm, predicted: 3.7 μm). Indeed, the SEM image shows a fairly uniformly dense film with a more porous layer of iron carbonate adjacent to the steel surface, as predicted. It should be noted that during the experiment <1 μm of steel was lost to the corrosion process.

Comparison Case #2

The next test of the model was to compare its performance using a different set of environmental conditions. It was particularly interesting to evaluate if the newly established relationship between the surface area-to-volume ratio and the porosity of the film depicted in Figure 3 would apply without adjustment what would build confidence in its generality. A second set of experiments used for verification was conducted under the same condition as the previous set (T = 80°C, pH 6.6, P_{CO_2} = 0.54 bar, v = 1 m/s) with the exception of the steel wool, which was not used, resulting in a much lower Fe^{2+} concentration. Using equilibrium calculations, based on pH 4.6 measured at the beginning of the experiment, it was estimated that the Fe^{2+} concentration was ≈5 ppm to 10 ppm throughout most of the experiment. The value of pH was adjusted to 6.6 by adding $NaHCO_3$—resulting in a bulk supersaturation S = 10 to 23 and a surface scaling tendency of SST = 0.25 to 0.47 prior to any film formation. Based on the high supersaturation, it was expected that some precipitation would occur; however, the low value of the surface scaling tendency suggested that the film could have trouble attaching to the surface.

The experiment was stopped after 2 days without achieving protective film formation. In Figure 7, measured and predicted corrosion rates were compared and both show that no protective films were formed after 48 h. The agreement is rather good given that no adjustment of the model was made. In Figure 8, the prediction showed that some precipitation occurred; however, the film layers adjacent to the rapidly corroding steel surface remained very porous

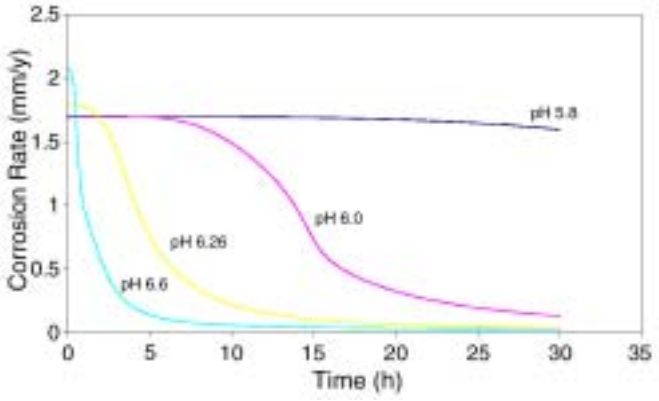

FIGURE 11. *Predicted effect of pH on the corrosion rate for T = 80°C, P_{CO_2} = 0.54 bar, $c_{Fe^{2+}}$ = 250 ppm, and v = 1 m/s. Corresponding film thickness and porosity are shown in Figure 12. Predicted supersaturation and scaling tendency are listed in Table 1.*

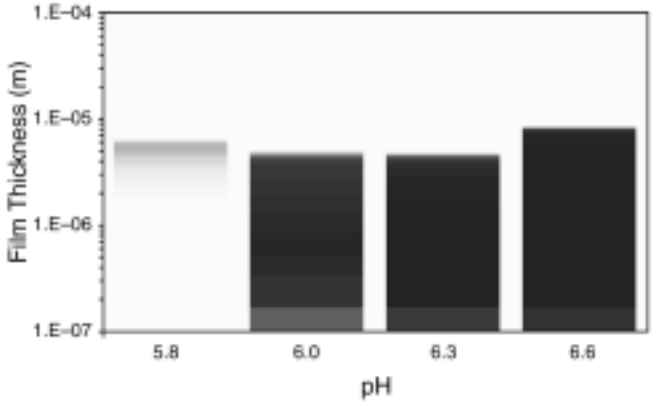

FIGURE 12. *Predicted film thickness and porosity as a function of pH after 30 h of exposure at T = 80°C, P_{CO_2} = 0.54 bar, $c_{Fe^{2+}}$ = 250 ppm, and v = 1 m/s. Black depicts a 100% dense (ε = 0) iron carbonate film and white means no film (ε = 1). The corresponding corrosion rate curves are shown in Figure 11. Predicted supersaturation and scaling tendency are listed in Table 1.*

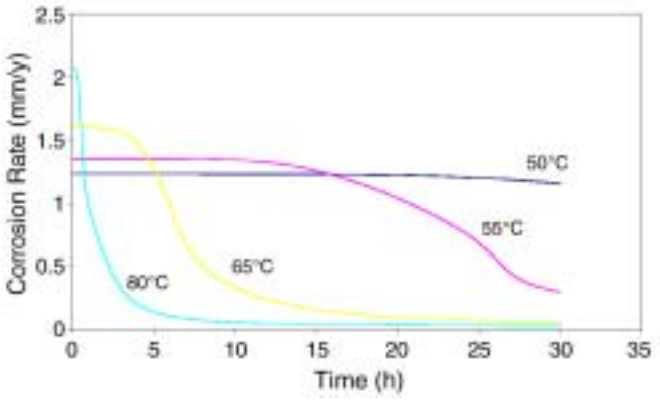

FIGURE 13. *Predicted effect of temperature on the corrosion rate for pH 6.6, P_{CO_2} = 0.54 bar, $c_{Fe^{2+}}$ = 250 ppm, and v = 1 m/s. Corresponding film thickness and porosity are shown in Figure 14. Predicted supersaturation and scaling tendency are listed in Table 2.*

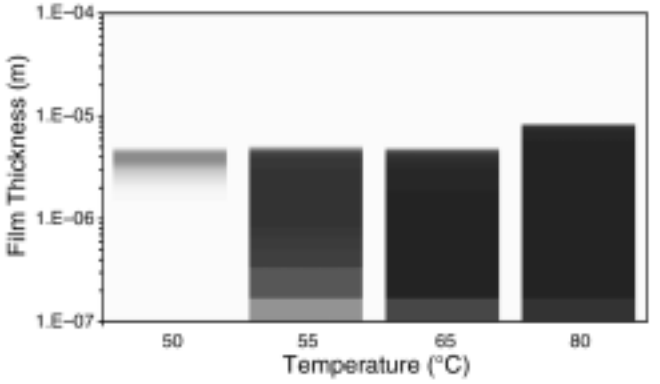

FIGURE 14. *Predicted film thickness and porosity as a function of temperature after 30 h of exposure at pH 6.6, P_{CO_2} = 0.54 bar, $c_{Fe^{2+}}$ = 250 ppm, and v = 1 m/s. Black depicts a 100% dense (ε = 0) iron carbonate film and white means no film (ε = 1). The corresponding corrosion rate curves are shown in Figure 13. Predicted supersaturation and scaling tendency are listed in Table 2.*

due to the undermining effect while a more dense film grew at some distance away from the steel surface. The same is shown in Figure 9, showing that a relatively dense film formed at ≈5 μm to 10 μm away from the surface after 48 h of exposure. Qualitatively this agreed well with the cross-sectional examination conducted using SEM, as shown in Figure 10, where a totally detached layer of iron carbonate can be seen ≈10 μm to 20 μm away from the steel surface. During the experiment, ≈10 μm of steel was lost to the corrosion process.

Clearly, one can be satisfied with the qualitative predictions obtained with the model. Not all of the predicted quantities agreed well enough with the experiments (e.g., film thickness), suggesting that some more fine-tuning is needed, requiring a new set of dedicated CO_2 corrosion experiments conducted under a variety of environmental conditions leading to iron carbonate film growth. This is a task for the immediate future.

PARAMETRIC TESTING

In this section the model will be used to predict CO_2 corrosion under broadly varying environmental conditions to establish its more general applicability. No direct comparisons with experiments will be made in this section; however, performance of the model will be contrasted against the general understanding of the CO_2 corrosion process in the presence of iron carbonate films. As shown in the previous section (Comparison Case #1), the model was successful in predicting CO_2 corrosion and film formation in an experiment conducted at T = 80°C, pH = 6.6, P_{CO_2} = 0.54 bar, $c_{Fe^{2+}}$ = 250 ppm, and v = 1 m/s. Therefore, this set of conditions will be used as a baseline case when varying the different parameters, one at a time.

Effect of pH

It was shown previously both experimentally[16] and computationally[17] that pH has a strong influence on the conditions leading to the formation of iron carbonate films. High-pH results in a decreased solubility of iron carbonate, increased supersaturation, and consequently higher precipitation rate and surface scaling tendency. In Table 1, the predicted supersaturation, scaling tendency, film thickness, and a corrosion rate after 30 h of exposure at various pH

TABLE 2

Predicted Supersaturation, Scaling Tendency, Film Thickness, and Corrosion Rate at Various Temperatures for pH 6.6, P_{CO_2} = 0.54 bar, $c_{Fe^{2+}}$ = 250 ppm, and v = 1 m/s

T in °C	Supersaturation (prior to any film formation)		Scaling Tendency (prior to any film formation)		Film Thickness[A] (after 30 h) in μm	Corrosion Rate[B] (after 30 h) in mm/y
	Surface	Bulk	Surface	Bulk		
50	562	245	0.43	0.19	4.9	1.16
55	675	290	0.76	0.32	5.1	0.3
65	969	387	2.22	0.87	5.1	0.06
80	1,595	576	9.70	3.35	8.4	0.03

[A] Film thickness as well as porosity are shown in Figure 14.
[B] Corresponding corrosion rate vs time curves are shown in Figure 13.

are shown. Judging by the high supersaturation alone, one could expect that protective film should form in all cases, given that the temperature is relatively high (80°C). However, the surface scaling tendency seems to suggest that protective film formation might be very difficult at pH 5.8 (as SST<1) and probably sluggish at pH 6.0 (SST ≈ 1). The predictions of the corrosion rate at varying pH confirmed this, as shown in Figure 11. At pH 5.8, the corrosion rate is not reduced by a significant amount after 30 h, reflecting the fact that a relatively porous, detached, and unprotective film formed, as shown in Figure 12. A clear trend can be observed in Figure 11—higher pH resulted in faster formation of more protective films, as expected. From Figure 12, one can deduce that as the pH was increased the resulting film was of similar thickness but progressively became more dense and protective, particularly in the vicinity of the steel surface.

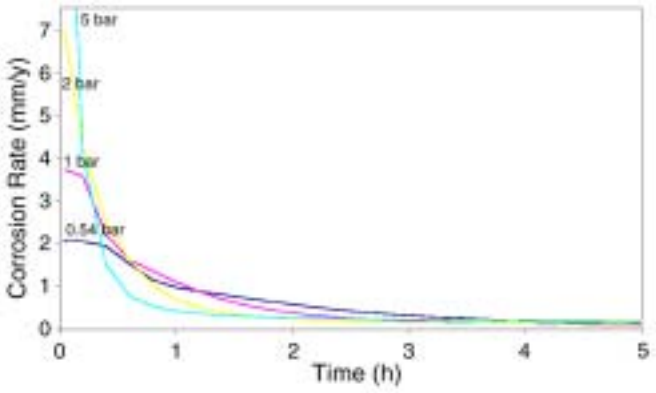

FIGURE 15. *Predicted effect of CO_2 partial pressure on the corrosion rate for T = 80°C, pH 6.6, $c_{Fe^{2+}}$ = 250 ppm, and v = 1 m/s. Corresponding film thickness and porosity are shown in Figure 16. Predicted supersaturation and scaling tendency are listed in Table 3.*

Effect of Temperature

It is known that increased temperature aids iron carbonate film formation by accelerating the kinetics of precipitation. The predicted temperature effect on CO_2 corrosion is illustrated in Figure 13 for the baseline case (temperatures <50°C are not shown as no film could be detected). Prior to any film formation, the corrosion rate increases with temperature as expected. While very protective films formed rapidly at 80°C, already at 65°C and 55°C the kinetics of film formation was much slower. At 50°C, it was so slow that only some very porous film formation can be detected. It is rather striking how under certain conditions a difference of 5°C can lead to two very different corrosion outcomes. At 55°C, iron carbonate films form, which offer good protection. At 50°C, there is a detached, porous layer of iron carbonate film, which offers little protection. Calculated data shown in Table 2 support this conclusion, where very high supersaturation is obtained at all temperatures; however, the surface scaling tendency is significantly smaller than unity, only at 50°C. By looking at Figure 14 it can be seen that the predicted film thickness does not vary much with temperature; however, the film formed at 55°C is more porous, particularly close to the metal surface as a result of the undermining effect than one formed at 65°C. At 80°C, a very dense and thick protective film is obtained.

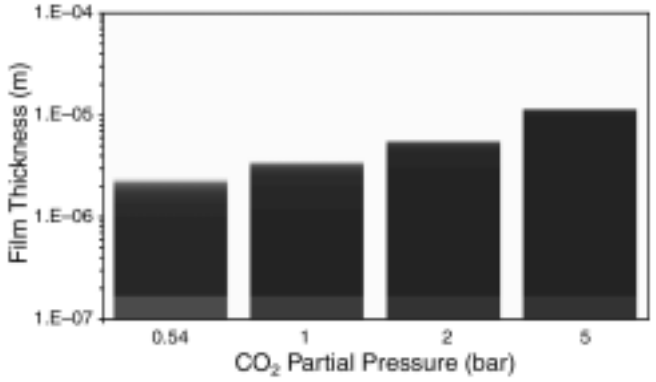

FIGURE 16. *Predicted film thickness and porosity as a function of CO_2 partial pressure after 5 h of exposure at T = 80°C, pH 6.6, $c_{Fe^{2+}}$ = 250 ppm, and v = 1 m/s. Black depicts a 100% dense (ε = 0) iron carbonate film and white means no film (ε = 1). The corresponding corrosion rate curves are shown in Figure 15. Predicted supersaturation and scaling tendency are listed in Table 3.*

TABLE 3

Predicted Supersaturation, Scaling Tendency, Film Thickness, and Corrosion Rate at Various CO_2 Partial Pressures for T = 80°C, pH 6.6, $c_{Fe^{2+}}$ = 250 ppm, and v = 1 m/s

P_{CO_2} in bar	Supersaturation (prior to any film formation)		Scaling Tendency (prior to any film formation)		Film Thickness[A] (after 5 h) in μm	Corrosion Rate[B] (after 5 h) in mm/y
	Surface	Bulk	Surface	Bulk		
0.54	1,595	576	9.70	3.35	2.5	0.14
1	3,078	1,069	10.77	3.59	3.5	0.11
2	5,881	2,142	11.75	4.13	5.6	0.12
5	11,800	5,422	12.26	5.66	11.4	0.2

[A] Film thickness as well as porosity are shown in Figure 16.
[B] Corresponding corrosion rate vs time curves are shown in Figure 15.

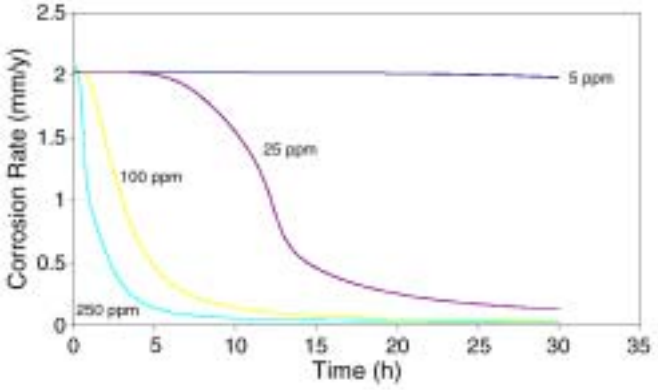

FIGURE 17. *Predicted effect of Fe^{2+} concentration on the corrosion rate for T = 80°C, pH 6.6, P_{CO_2} = 0.54 bar, and v = 1 m/s. Corresponding film thickness and porosity are shown in Figure 18. Predicted supersaturation and scaling tendency are listed in Table 4.*

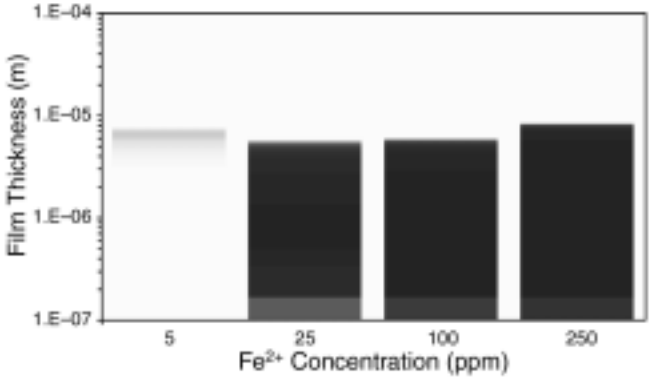

FIGURE 18. *Predicted film thickness and porosity as a function of Fe^{2+} ion concentration after 30 h of exposure at T = 80°C, pH 6.6, P_{CO_2} = 1 bar, and v = 1 m/s. Black depicts a 100% dense (ε = 0) iron carbonate film and white means no film (ε = 1). The corresponding corrosion rate curves are shown in Figure 17. Predicted supersaturation and scaling tendency are listed in Table 4.*

Effect of CO_2 Partial Pressure

In the case of film-free CO_2 corrosion, an increase of CO_2 partial pressure (P_{CO_2}) typically leads to an increase in the corrosion rate. However, when other conditions are favorable for formation of iron carbonate films, increased P_{CO_2} can help. At a constant pH, higher P_{CO_2} leads to an increase in CO_3^{2-} concentration and a higher supersaturation (given the pH is high enough)—what accelerates precipitation and film formation. The effect of P_{CO_2} on the corrosion rate in the presence of iron carbonate precipitation is illustrated in Figure 15 for the baseline case. Prior to film formation, increased P_{CO_2} leads to a rapid rise in corrosion rate. However, protective films form rapidly in all cases, even for the lowest, P_{CO_2} = 0.54 bar (given the pH 6.6 and high Fe^{2+} concentration). An increase in P_{CO_2} leads to formation of even more protective films—and this happens faster. Data are presented only for the first 5 h of corrosion as very low, almost indistinguishable corrosion rates are obtained beyond. One could expect such behavior just by looking at the high supersaturations and scaling tendencies shown in Table 3. By inspecting Figure 16, it can be concluded that somewhat denser and clearly thicker films form at higher P_{CO_2}.

Effect of Fe^{2+} Concentration

The concentration of Fe^{2+} ions in the solution ($c_{Fe^{2+}}$) is another important factor that contributes to film formation. The increase of $c_{Fe^{2+}}$ results in higher supersaturation, which consequently accelerates the precipitation rate and leads to higher surface scaling tendency. In Figure 17, the effect of $c_{Fe^{2+}}$ on the rate of corrosion rate reduction due to iron carbonate film formation is shown for the baseline case. The $c_{Fe^{2+}}$ does not affect the corrosion rate if there is no iron carbonate film (at t = 0). At $c_{Fe^{2+}}$ = 5 ppm, supersaturation is achieved; however, the surface scaling tendency is much less than unity (Table 4), and one cannot expect protective films to form. This is confirmed as the corrosion rate is not reduced significantly even after 30 h (Figure 17). The iron carbonate film that forms is very porous and unprotective (Figure 18 but also the Comparison Case #2—Figure 7 through Figure 10). At higher concentrations, more protective films form, as shown in Figures 17 and 18.

TABLE 4

Predicted Supersaturation, Scaling Tendency, Film Thickness, and Corrosion Rate at Various Fe^{2+} Concentrations for T = 80°C, pH 6.6, P_{CO_2} = 0.54 bar, and v = 1 m/s

$c_{Fe^{2+}}$ in ppm	Supersaturation (prior to any film formation)		Scaling Tendency (prior to any film formation)		Film Thickness[A] (after 30 h) in μm	Corrosion Rate[B] (after 30 h) in mm/y
	Surface	Bulk	Surface	Bulk		
5	51	11	0.27	0.05	7.1	1.98
25	185	58	1.1	0.32	5.7	0.13
100	671	230	3.90	1.31	6.0	0.04
250	1,595	576	9.70	3.35	8.4	0.03

[A] Film thickness as well as porosity are shown in Figure 18.
[B] Corresponding corrosion rate vs time curves are shown in Figure 17.

Effect of Velocity

Higher velocity is directly associated with higher turbulence and more effective mixing in the solution. This affects both the corrosion rate of the bare steel surface and the precipitation rate of iron carbonate. Prior to any film formation, high velocity leads to increased corrosion rates (Figure 19) as the transport of cathodic species toward the steel surface is enhanced by turbulent transport. At the same time, the transport of Fe^{2+} ions away from the steel surface is also increased, leading to a lower concentration of Fe^{2+} ions at the steel surface. This results in a lower surface supersaturation and slower precipitation rate (Table 5). Both effects contribute to less protective films being formed at high velocities. Interestingly, the model suggests that somewhat thicker films form at higher velocities; however, they are more porous particularly close to the metal surface (Figure 20). This behavior could clearly be termed flow-accelerated corrosion (FAC) even if no film dissolution or mechanical erosion is involved.

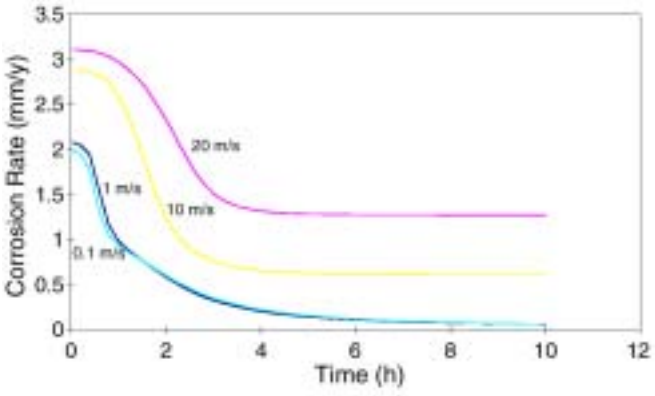

FIGURE 19. *Predicted effect of velocity on the corrosion rate for T = 80°C, pH 6.6, P_{CO_2} = 1 bar, and $c_{Fe^{2+}}$ = 250 ppm. Corresponding film thickness and porosity are shown in Figure 20. Predicted supersaturation and scaling tendency are listed in Table 5.*

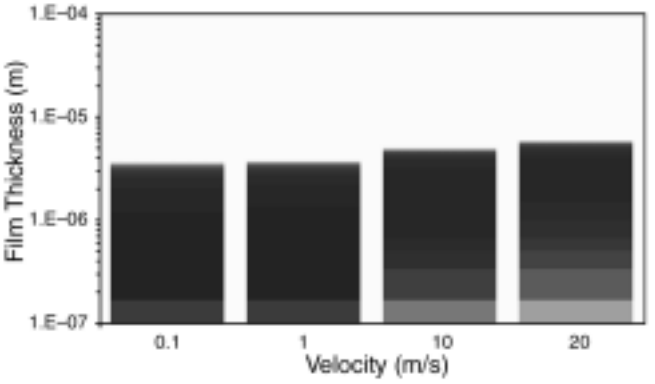

FIGURE 20. *Predicted film thickness and porosity as a function of velocity after 10 h of exposure at T = 80°C, pH 6.6, P_{CO_2} = 1 bar, and $c_{Fe^{2+}}$ = 250 ppm. Black depicts a 100% dense (ε = 0) iron carbonate film and white means no film (ε = 1). The corresponding corrosion rate curves are shown in Figure 19. Predicted supersaturation and scaling tendency are listed in Table 5.*

CONCLUSIONS

❖ A mechanistic model of iron carbonate film growth in CO_2 corrosion of carbon steel was created and coupled with the overall corrosion prediction model. The model relies on accurate prediction of the solution chemistry at the metal surface. It includes two principle mechanisms that determine the kinetics of growth and the resulting morphology of the iron carbonate films: precipitation and undermining of the film by ongoing corrosion. The morphology is described by the distribution of porosity throughout the film.

❖ The model is capable of predicting the kinetics of iron carbonate film growth, the change in morphology of the film with respect to space and time, as well as the resulting corrosion rate time evolution.

❖ The model has been successfully calibrated against limited experimental data. Further adjustment of the model will be done as more accurate data on CO_2 corrosion in the presence of iron carbonate films emerge.

❖ Parametric testing of the model has been done to gain insight into the effect of various environmental parameters on iron carbonate film formation. The trends shown in the predictions agreed well with the general understanding of the CO_2 corrosion process in the presence of iron carbonate films.

TABLE 5

Predicted Supersaturation, Scaling Tendency, Film Thickness, and Corrosion Rate at Various Velocities for T = 80°C, pH 6.6, P_{CO_2} = 0.54 bar, and $c_{Fe^{2+}}$ = 250 ppm

V in m/s	Supersaturation (prior to any film formation)		Scaling Tendency (prior to any film formation)		Film Thickness[A] (after 10 h) in μm	Corrosion Rate[B] (after 10 h) in mm/y
	Surface	Bulk	Surface	Bulk		
0.1	1,770	576	10.6	3.4	3.5	0.06
1	1,595	576	9.70	3.35	3.7	0.058
10	790	576	3.24	2.36	5.1	0.6
20	686	576	2.6	2.16	5.9	1.27

[A] Film thickness as well as porosity are shown in Figure 20.
[B] Corresponding corrosion rate vs time curves are shown in Figure 19.

❖ The present model confirms that the concept of scaling tendency is a good tool for predicting the likelihood of protective iron carbonate film formation. It was found that protective films formed when the surface scaling tendency was equal or larger than unity, otherwise porous and unprotective film formed irrespective of the level of supersaturation. If the bulk scaling tendency is used, the critical value is 0.6 to 0.7, which is close to the experimentally observed value by van Hunnik, et al.[4]

ACKNOWLEDGMENTS

During this work, J. Lee was supported by an Australian Postgraduate Award and a scholarship from the Mechanical Engineering Department, University of Queensland, Australia. The authors are grateful for many useful comments and discussions with A. Dugstad and R. Nyborg from IFE, Norway, and M. Nordsveen from Scandpower, Norway, which helped in creating this model as it stands today.

REFERENCES

1. S. Nešić, M. Nordsveen, R. Nyborg, A. Stangeland, "A Mechanistic Model for CO_2 Corrosion with Protective Iron Carbonate Films," CORROSION/2001, paper no. 01040 (Houston, TX: NACE International, 2001).
2. J.S. Newman, Electrochemical Systems, 2nd ed. (Englewood Cliffs, NJ: Prentice Hall, 1991).
3. J.T. Davies, Turbulence Phenomena (London, U.K.: Academic Press, 1972).
4. E.W.J. van Hunnik, B.F.M. Pots, E.L.J.A. Hendriksen, "The Formation of Protective $FeCO_3$ Corrosion Product Layers in CO_2 Corrosion," CORROSION/96, paper no. 6 (Houston, TX: NACE, 1996).
5. J.W. Mullin, Crystallization, 3rd ed. (Oxford, U.K.: Oxford, 1993).
6. I. Nainville, A. Lemarchand, J.P. Badiali, Electrochim. Acta 41, 11/12 (1996): p. 1,855.
7. M. Lafage, V. Russier, J.P. Badiali, J. Electroanal. Chem. 450 (1998): p. 203.
8. A. Taleb, J. Stafiej, A. Chausse, R. Messina, J.P. Badiali, J. Electroanal. Chem. 500 (2001): p. 554.
9. M.L. Johnson, M.B. Tomson, "Ferrous Carbonate Precipitation Kinetics and Its Impact on CO_2 Corrosion," CORROSION/91, paper no. 268 (Houston, TX: NACE, 1991).
10. P. Nakayama, F. Kuwahara, "Numerical Modeling of Convective Heat Transfer in Porous Media Using Microscopic Structures," Handbook of Porous Media (New York, NY: Marcel Dekker Publication, 1995).
11. L. Latour, P. Mitra, R. Kleinberg, C. Sotak, J. Magn. Res., Series A 101 (1993): p. 342.
12. K. Hoffmann, S. Chiang, "Computational Fluid Dynamics for Engineers—Volume 1," 4th print (Kansas: Engineering Education System, 1997).
13. B.P. Leonard, Comput. Methods Appl. Mech. Eng. 19 (1979): p. 59.
14. B. Koren, "A Robust Upwind Discretization Method for Advection, Diffusion, and Source Terms," Numerical Methods for Advection-Diffusion Problems (Braunschweig: Vieweg, 1993), p. 117.
15. S. Nešić, J. Postlethwaite, S. Olsen, Corrosion 52 (1996): p. 280.
16. A. Dugstad, "The Importance of $FeCO_3$ Supersaturation on the CO_2 Corrosion of Carbon Steels," CORROSION/92, paper no. 14 (Houston, TX: NACE, 1992).
17. S. Nešić, M. Nordsveen, R. Nyborg, A. Stangeland, Corrosion 59, 6 (2003): p. 489.